Rare-earth energy levels and magnetic properties of $HoPO_4$ and $ErPO_4$

1993 J. Phys.: Condens. Matter 5 5121

(http://iopscience.iop.org/0953-8984/5/29/009)

J. Phys.: Condens. Matter 5 (1993) 5121–5140. Printed in the UK

Rare-earth energy levels and magnetic properties of $HoPO_4$ and $ErPO_4$

C-K Loong†, L Soderholm†, J P Hammonds†, M M Abraham‡, L A Boatner‡ and N M Edelstein§

† Intense Pulsed Neutron Source and Chemistry Division, Argonne National Laboratory, Argonne, IL 60439-4814, USA
‡ Solid State Division, Oak Ridge National Laboratory, Oak Ridge, TN 37831-6056, USA
§ Chemical Sciences Division, Lawrence Berkeley Laboratory, Berkeley, CA 94720, USA

Received 12 January 1993

Abstract. The static and dynamic magnetic responses of $HoPO_4$ and $ErPO_4$ have been studied by means of neutron spectroscopy and magnetic susceptibility measurements. The inelastic neutron scattering spectra exhibit well-defined transitions characteristic of crystal-field excitations of the rare-earth ions. The data were analysed using a Hamiltonian that included atomic free-ion and crystal-field interactions for an f^N configuration (N = 10 and 11 for Ho^{3+} and Er^{3+}, respectively). Using the free-ion parameters derived from optical spectroscopy of the corresponding rare-earth ions diluted in a YPO_4 host, crystal-field parameters for both $HoPO_4$ and $ErPO_4$ were obtained. A comparison of the neutron data with optical absorption and both non-resonance and resonance Raman scattering measurements has been made. The derived crystal-field-level structure provides a basis for explaining the low-temperature magnetic properties of both compounds. The calculated and measured paramagnetic susceptibilities agree well for $HoPO_4$ and $ErPO_4$ in the temperature range of 5–300 K. The highly anisotropic, saturated magnetization of the ground doublet in $HoPO_4$ may act as a 'bootstrap' for a long-range magnetic ordering of the moments parallel to the c-axis at low temperatures. The nearly spherically symmetric moments of the low-lying Kramers doublets of $ErPO_4$, however, tend to couple less effectively via exchange interactions. The effective exchange field in antiferromagnetic $HoPO_4$, as estimated based on the crystal-field-level scheme and a molecular-field approximation, is found to be in good agreement with that reported from a specific-heat analysis. The paramagnetic specific heat, spectroscopic splitting g-factors of the low-lying doublet states, and saturated moments for $HoPO_4$ and $ErPO_4$ obtained from the present study are applicable to interpreting specific heat, hyperfine interaction, EPR, and neutron diffraction measurements.

1. Introduction

Mixed natural rare-earth orthophosphates, RPO_4 (R = rare earths), form the minerals monazite (R = La–Gd) and xenotime (R = Tb–Lu). Pure crystalline forms of these compounds can be synthesized by controlled precipitation techniques, and single crystals of the materials can be grown by means of flux methods. The high melting temperatures (about 2000 °C), structural and chemical stability, and long-term corrosion resistance of the RPO_4 compounds make these substances attractive for applications as high-temperature components and nuclear waste storage media (Boatner *et al* 1980, 1981, Hikichi and Nomura 1987). The optical and magnetic properties of the rare-earth ions in RPO_4 hosts, including their rare-earth-activated luminescence, magnetic phase transitions, and Jahn–Teller effects, have also prompted numerous fundamental experimental and theoretical

investigations. Increasing our knowledge of the rare-earth energy levels and wavefunctions in RPO_4 compounds is, of course, essential to understanding both the bulk and microscopic properties of these materials.

We have recently initiated a systematic study of magnetic excitations in the stoichiometric RPO_4 series using neutron spectroscopy. The motivation for this investigation is manifold, since neutron-scattering data also provide information on the low-lying rare-earth crystal-field states which complements the high-energy data obtained by optical spectroscopy. In the particular case of $TmPO_4$, we have previously demonstrated that a combined analysis of neutron and optical data provides a satisfactory characterization of the energy splitting of the f^{12} configuration of Tm^{3+} (Loong *et al* 1993a). The standard method of data interpretation in this case is based on an empirical Hamiltonian that consists of a spherically symmetric free-ion part and a non-spherically symmetric crystal-field part. The crystal-field portion of the Hamiltonian, H_{CF}, is expressed in terms of one-electron effective-tensor operators, each of which is associated with a crystal-field parameter, summed over the unpaired f electrons (or holes in the case of a more than half-filled shell) in an f^N configuration. Effects of electronic orbital and spin correlation on the crystal-field interactions are usually ignored. In general this method is capable of producing a satisfactory classification of the energy levels over a wide energy range (0 to $\simeq 20\,000$ cm^{-1}) for many f-electron systems. In the case of Tm^{3+} in an $LuPO_4$ host, a root-mean-square energy deviation of 10 cm^{-1} between the calculated and observed energies up to about 38 000 cm^{-1} has been achieved (Becker *et al* 1984).

In the present work, neutron-scattering measurements of crystal-field transitions within the R^{3+} ground multiplet and associated data analysis for pure $HoPO_4$ and $ErPO_4$ have been performed. Optical absorption spectra of the transitions $^5I_8 \rightarrow {}^5I_7$ and $^5I_6$ (5000–12 000 cm^{-1}) and $^5I_8 \rightarrow {}^3K_7$ and $^3H_6$ (26 000–28 000 cm^{-1}) of Ho^{3+} in $HoPO_4$ have been measured and analysed previously by Bischoff *et al* (1991), and Enderle *et al* (1990), respectively. Recognizing the importance of electron-correlation effects on the crystal-field interactions in the characterizations of the high-energy levels, Pilawa (1991a, b) has recently extended the analysis of the $HoPO_4$ data using the formalism of correlated crystal-field theory. Since the transitions within the Ho^{3+} $^5I_8$ ground multiplet have not been included in the optical studies, it is desirable to determine the crystal-field-level structure of the ground multiplet by neutron inelastic scattering. It is also of interest to compare the energy-level structure of $HoPO_4$ and $TmPO_4$ with that of $ErPO_4$. The latter compound has an odd ($N = 11$) number of f electrons so that the symmetry of all the states cannot be lower than a Kramers doublet. Furthermore, a near coincidence in energy between the argon ion laser excitation line at 488.0 nm and Er^{3+}, $^4I_{15/2} \rightarrow {}^4F_{7/2}$ transitions in $ErPO_4$ has permitted resonant electronic Raman scattering measurements to be carried out in which Becker *et al* (1985b, 1986), determined all of the energy levels within the ground $^4I_{15/2}$ multiplet. A neutron-scattering study of the crystal-field excitations and their transition strengths in $ErPO_4$ affords an intriguing comparison with the Raman-scattering results and also contributes to a determination of the crystal-field parameters.

The present study of the RPO_4 series is also motivated by the rich variety of magnetic properties exhibited by this system. In the temperature range of 0–300 K, coupling of the low-lying crystal-field states, phonons, and local deformations of the lattice gives rise to different forms of anomalous behaviour. For example, strong 4f-electron–phonon coupling effects in $YbPO_4$ have been observed recently in a Raman-scattering study reported by Becker *et al* (1992). The temperature dependence of the lattice parameters and the Young's modulus of RPO_4 (R = Tb–Yb) has been measured and studied theoretically in terms of magnetoelastic and Jahn–Teller interactions by Sokolov *et al* (1991, 1992). At low

temperatures ($T < 4$ K), the rare-earth crystal-field ground state (and the very low-energy states that remain thermally populated) has important consequences for the nature of the magnetocrystalline anisotropy and magnetic interactions with other ions. The rare-earth magnetic moments in $TbPO_4$, $HoPO_4$, and $DyPO_4$ order antiferromagnetically at 2.2, 1.4, and 3.4 K, respectively (Lee *et al* 1971, Cooke *et al* 1973, Wright and Moss 1969). Knowing the ground-state properties of the rare-earth ions, many of the low-temperature properties of these three compounds (e.g. the magnetic susceptibility, heat capacity, and optical absorption spectrum) can be described by simple models such as a three-dimensional Ising lattice (see, for example, the review by De Jongh and Miedema (1974)). The Néel temperatures T_N for $ErPO_4$, $TmPO_4$, and $YbPO_4$ have not been determined, but for $ErPO_4$, T_N is expected to be about 0.5 K (Will *et al* 1971). Obviously, a characterization of the rare-earth energy levels and wavefunctions in RPO_4 represents a prerequisite for understanding the single-site magnetic properties as well as the cooperative interactions.

A systematic comparison of the energy levels of the rare-earth ions in RPO_4 with those of the same ions in a different host (such as R^{3+} ions in LaF_3) is useful in assessing the extent to which the rare-earth free-ion parameters can vary among different host materials. Such a comparison also facilitates a model analysis of possible intrinsic relationships that connect the crystal-field parameters of R^{3+} ions in different materials. In particular, it is of interest to determine the effects, if any, that result from the adoption of the LaF_3 parameters in an analysis of the crystal-field spectra of the rare-earth copper oxide superconductors $RBa_2Cu_3O_7$ and $R_{2-x}Ce_xCuO_4$ (Soderholm *et al* 1991, 1992, Loong and Soderholm 1992a, Goodman *et al* 1991). The spectroscopic parameters for these superconductors cannot be obtained by optical spectroscopy because of the opacity of the materials. The relationship between the crystal-field parameter sets for $PrBa_2Cu_3O_7$ and Pr_2CuO_4 has, however, been examined previously by employing the superposition model (Loong and Soderholm 1992b).

The present article is organized as follows. In section 2, the methods of sample preparation and structural characterization and the neutron-scattering procedures are discussed. The experimental data are subsequently presented in section 3, followed in section 4 by the crystal-field analysis and a comparison of the results with those obtained by other workers using different experimental techniques. The effect of the crystal-field splittings in determining the magnetic properties of $HoPO_4$ and $ErPO_4$ are discussed in section 5. A preliminary account of the $ErPO_4$ results and a detailed paper dealing with spectroscopic studies of $TmPO_4$ have been presented previously (Loong *et al* 1993a, b).

2. Experimental details

Polycrystalline samples of $HoPO_4$ and $ErPO_4$ of about 100 g each, were prepared by coprecipitation of the subject rare-earth oxide and ammonium hydrogen phosphate in molten urea followed by a calcination at 800 °C to remove the urea (Abraham *et al* 1980). Both samples, in the form of a fine powder, were examined by x-ray diffraction and were found to exhibit the appropriate tetragonal zircon structure. No impurity phases were observed within the experimental uncertainty. The powder samples were then pressed into pellets and annealed at 1200 °C in air for 24 h, since such heat treatments are known to promote grain growth and improve the crystalline quality (Abraham *et al* 1980). The annealed samples were characterized by neutron powder diffraction using the general-purpose power diffractometer (GPPD) at the intense pulsed neutron source (IPNS) of Argonne National Laboratory. The observed powder patterns confirm the single-phase zircon structure of pure $HoPO_4$ and $ErPO_4$, as reported by Milligan *et al* (1983a). *R*-factors of 6.7 and 5.8%

were obtained for $HoPO_4$ and $ErPO_4$, respectively, in a Rietvelt analysis of the neutron powder data. All of the results described in the present paper were obtained using these heat-treated samples.

The present neutron-scattering experiments were conducted using the high-resolution medium-energy chopper spectrometers (HRMECS) at IPNS. This pulsed-neutron source, equipped with cold moderators, provides a large flux of cold-to-epithermal neutrons that are useful for the study of the small crystal-field splittings and high-energy phonons characteristic of rare-earth orthophosphates. In general, the energy resolution ΔE (full width at half-maximum) of the HRMECS spectrometer varies between 2 and 4% of the incident neutron energy E_0 over the neutron energy-loss region, $E = E_0 - E_1 > 0$ (where E_1 is the scattered neutron energy) (Loong *et al* 1987). For example, $\Delta E \simeq 0.6$ meV and 2.5 meV at $E = 5$ meV if E_0 is 20 and 80 meV, respectively. In addition, the wide-scattering-angle detector banks collect data over a large range of wave vectors Q. In the absence of a spin-polarization analysis of the incident and scattered neutrons, the experimentally observed intensity includes the scattering of neutrons by magnetic electrons as well as by atomic nuclei. For polycrystalline samples, the nuclear scattering consists of an elastic peak at zero energy transfer and a diffuse backgound that is mainly due to phonon scattering. At small $Q(< 4\ \text{Å}^{-1})$ values and at low temperatures, the phonon contributions are small; therefore, crystal-field peaks can easily be identified. At larger Q values or at elevated temperatures, phonon scattering usually dominates the measured spectrum. Thus, studying the Q and temperature dependence of the measured intensities helps in discerning the origin of the scattering processes.

In order to observe and resolve the crystal-field peaks as a function of temperature over the energy range of 0–150 meV, we have conducted experiments with the following conditions for the incident neutron energies and sample temperatures (E_0, T): for $HoPO_4$, 20 meV, 15, 50, 100, 150 and 250 K; 40 meV, 15 and 100 K; 80 meV, 15, 100 and 160 K; and 200 meV, 15 and 250 K; and for $ErPO_4$, 20 and 40 meV, 15, 30 and 296 K; 80 and 200 meV, 15 K. In order to obtain information regarding the elastic and inelastic contributions from nuclear scattering, we have also measured the energy spectra of the isostructural but non-magnetic compound $LuPO_4$ at 15 K using HRMECS with $E_0 = 60$ and 200 meV. 'Empty-container' and absorber runs were used to correct for the background scattering and to evaluate sample attenuation effects. Measurements of the elastic incoherent scattering from a vanadium standard provided detector calibration and intensity normalization.

3. Results

The magnetic scattering of thermal neutrons arises from an interaction of the neutron magnetic moment with the convection and spin current of the scatterer. Such a weak interaction does not involve excited intermediate states of the system and only requires a first-order perturbation treatment (i.e. the Born approximation). For a system of non-interaction ions with f^N orbitals, the convection and spin-current operator is related to the total (orbital and spin) angular momentum operator of N equivalent f electrons, which can be expanded in multipole fields using spherical tensor techniques (Stassis and Dechman, 1975, 1976). For thermal-neutron scattering at small wave vectors, as is the usual case, only magnetic-dipole transitions need to be considered (Lovesey 1984). Ignoring dynamic coupling of the spins and the lattice, the magnetic scattering from an assembly of N non-interacting rare-earth ions at a temperature T can be expressed in terms of the double

partial-differential scattering cross section as

$$\frac{d^2\sigma}{d\Omega dE} = N(k_f/k_i)\tfrac{1}{4}(\gamma r_0)^2 g_J^2 S(\boldsymbol{Q}, E) \tag{1}$$

where the scattering function $S(\boldsymbol{Q}, E)$ is expressed as

$$S(\boldsymbol{Q}, E) = f^2(\boldsymbol{Q})\exp[-2W(\boldsymbol{Q})]\sum_{n,m}\frac{\exp(-E_n/k_BT)}{Z}|\langle n|J_\perp|m\rangle|^2\delta(E_n - E_m - E). \tag{2}$$

In the above equations, $\hbar\boldsymbol{Q}$ and E are the momentum and energy transfer, respectively, $k_i(k_f)$ is the initial (final) neutron wave vector, γ is the neutron magnetic moment in units of nuclear Bohr magnetons, r_0 is the electron classical radius, g_J is the Landé g factor, $f(\boldsymbol{Q})$ is the ionic magnetic form factor, Z is the partition function, and $\exp[-2W(\boldsymbol{Q})]$ is the Debye–Waller factor. In general, the ith crystal-field state $\langle i|$ at an energy E_i is a mixture of $|J, M\rangle$ states including those from higher-J multiplets, and $J_\perp$ is the component of the total angular-momentum operator perpendicular to $\boldsymbol{Q}$. For experiments using polycrystalline samples and unpolarized neutrons, only the modulus of $\boldsymbol{Q}$ is retained so that

$$|\langle|J_\perp|\rangle|^2 = \tfrac{2}{3}(|\langle|J_x + J_y|\rangle|^2 + |\langle|J_z|\rangle|^2). \tag{3}$$

The spectroscopic splitting g-factors with respect to a quantization z-axis for a doublet states of effective spin $\frac{1}{2}$ are given by

$$|g_\parallel| = 2\langle\Gamma_i^+|L_z + 2S_z|\Gamma_i^+\rangle \tag{4a}$$

$$|g_\perp| = 2\langle\Gamma_i^+|L_x + 2S_x|\Gamma_i^-\rangle = 2\langle\Gamma_i^+|L_y + 2S_y|\Gamma_i^-\rangle \tag{4b}$$

where $|\Gamma_i^+\rangle$ and $|\Gamma_i^-\rangle$ are the doublet wavefunctions obtained from diagonalization of the Hamiltonian matrix under the scheme of intermediate coupling and $\boldsymbol{L}$ ($\boldsymbol{S}$) is the orbital (spin) momentum operator. In units of $Å^{-1}$, Q can be calculated from the scattering kinematics, namely, from the expression:

$$Q^2 = (1/2.0717)[2E_0 - E - 2\sqrt{E_0(E_0 - E)}\cos\phi] \tag{5}$$

where ϕ is the scattering angle, and E_0 and E are in meV. (1 meV is equivalent to 8.066 cm^{-1}. These two units of energy will be used interchangeably in the paper.) Neutron-energy-loss processes correspond to the case $E = E_n - E_m > 0$. At low temperatures, these scattering processes dominate because the Boltzmann factors $\exp(-E_n/k_BT)$ in equation (2) are small except for the ground state. At elevated temperatures, both neutron energy-loss and energy-gain ($E < 0$) processes are observed in the measured spectra.

The crystal-field transitions that occur via magnetic-dipole interactions in a neutron experiment are governed by a selection rule (Lovesey 1984) in which the Kronecker product of the irreducible representations of the initial and final crystal-field states and the angular-momentum operator under the point-group symmetry of the rare-earth ion (i.e. $\Gamma_n \otimes \Gamma_{J_{z,\perp}} \otimes \Gamma_m$) must contain the unit representation Γ_1. This condition differs from the normal electric-dipole selection rules for optical spectroscopy, and therefore, may provide information on the energy levels that is inaccessible by optical techniques.

3.1. $HoPO_4$

$HoPO_4$ and $ErPO_4$ crystallize in the tetragonal zircon structure (space group $I4_1/amd$) which is the crystal structure common to the mineral xenotime or YPO_4 (Milligan *et al* 1983a, b). The rare-earth ions are located at sites of D_{2d} point-group symmetry. In the case of $HoPO_4$, the Ho^{3+}: $^5I_8$ ground multiplet is split by the crystal field into nine singlets, $3\Gamma_1 + 2\Gamma_2 + 2\Gamma_3 + 2\Gamma_4$, and four doublets, $4\Gamma_5$. The allowed transitions are $\Gamma_1 \leftrightarrow \Gamma_2, \Gamma_1 \leftrightarrow \Gamma_5, \Gamma_2 \leftrightarrow \Gamma_5, \Gamma_3 \leftrightarrow \Gamma_4, \Gamma_3 \leftrightarrow \Gamma_5, \Gamma_4 \leftrightarrow \Gamma_5$, and $\Gamma_5 \leftrightarrow \Gamma_5$. A complex crystal-field excitation spectrum is expected because many of the allowed transitions may be too weak to observe or too close in energy to resolve experimentally. Therefore, it is important to collect data over a wide range of temperatures so that changes in the overall spectrum, as higher-lying energy levels become populated with increasing temperature, can be analysed collectively. The observed scattering functions summed over scattering angles of 3–19° are shown in the upper panels of figures 1 and 2. The 20 meV (figure 1) and 40 meV (figure 2) runs are optimized for measurements of transitions in the regions of 0–15 and 15–30 meV, respectively. The phonon background is small (< 10%), particularly at low temperatures, therefore the spectra can be accounted for by magnetic scattering. A strong magnetic–elastic component at zero energy transfer, superimposed on the nuclear elastic scattering, can be identified by comparing the elastic peak intensity with the expected nuclear elastic cross section as calibrated by the vanadium standard runs. Thus, it follows that the Ho^{3+} ground state is a magnetic Γ_5 doublet. The observed inelastic features can be divided into two groups: (i) the sharp lines at 8.4, 9.8 and 23 meV (labelled A, B, D and E in figures 1 and 2) and a shoulder at 20 meV (C); and (ii) the overlapping peaks in the 2–6 meV (F–H, J) and 13–20 meV (L, N, O) regions and a weak shoulder at 26 meV (I). The intensities of the features in the first group decrease with increasing temperature whereas those of the second group increase with increasing temperature. This temperature dependence of the intensities indicates that peaks A–E originate from crystal-field excitations from the ground states, and the others are due to transitions from low-lying excited states. De-excitations from thermally occupied states to the ground states are also observed as neutron energy-gain processes ($E < 0$) in figures 1 and 2, but they are not well resolved because of the poor resolution in this region. The observed transition yields information regarding the energies of all the crystal-field states except the highest Γ_1 state within the ground multiplet. A comparison of the observed scattering functions as a function of temperatures with those calculated by equation (2) provides a goodness-of-fit test of the crystal-field model.

3.2. $ErPO_4$

The Er^{3+} $^4I_{15/2}$ ground multiplet of $ErPO_4$ is split by the tetragonal crystal field into four Γ_6 and four Γ_7 Kramers doublets. Excitations (or de-excitations) between any two doublet states and elastic scattering within a doublet are allowed by the selection rules for magnetic-dipole transitions in a neutron scattering experiment. Figures 3 and 4 show the observed neutron spectra obtained with incident energies of 20, 40, and 80 meV. Sharp crystal-field peaks labelled B–G, and weak, unresolved crystal-field features H–K are observed at low temperatures. The peak A at zero energy consists of nuclear elastic scattering and crystal-field transitions within the doubly degenerate ground states. Peaks B′, C′ and B, C represent the de-excitation (neutron energy-gain) and the excitation (neutron energy-loss) processes, respectively, of the same crystal-field transitions. The peaks D, E, F and G originate from thermally occupied excited states, as indicated by the temperature dependence of their intensities. These observed features can be assigned to crystal-field transitions involving

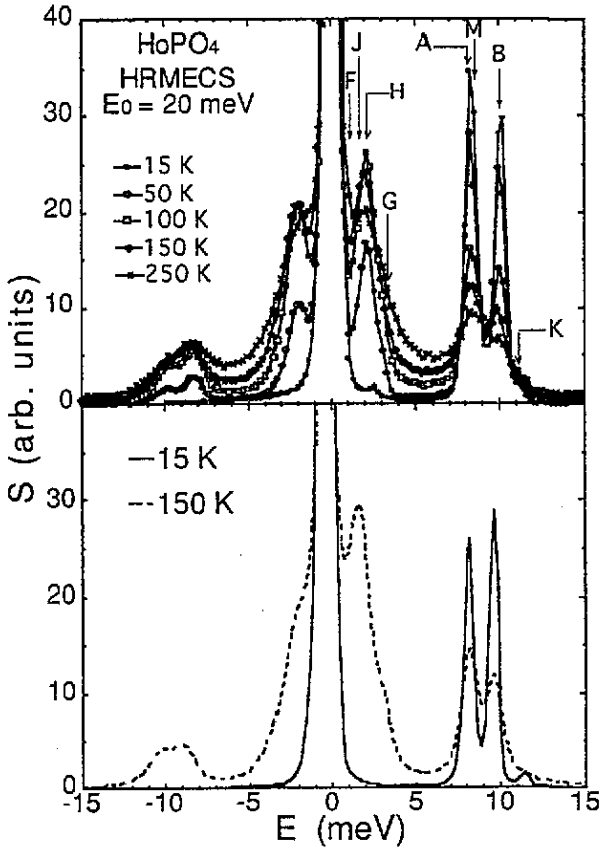

Figure 1. Upper panel: the measured total scattering functions for $HoPO_4$ at 15, 50, 100, 150 and 250 K with neutron incident energy of 20 meV. The curves are guides to the eye. The labelled peaks correspond to crystal-field transitions in figure 6. Lower panel: the calculated scattering functions for crystal-field transitions for $HoPO_4$ at 15 and 150 K. The assumed widths of the Lorentzian functions for crystal-field transitions at 15 and 150 K are 1 and 6 cm^{-1}, respectively. The calculated spectra have been convoluted with the instrumental resolution function (see text).

the seven lowest doublets within the ground multiplet. The intensities of transitions from the ground state (peaks A–C) decrease significantly at room temperature as expected, while unresolved crystal-field excitations from thermally populated states and phonons emerge, forming a diffuse background (figure 3). The broadening of the crystal-field peaks at high temperatures is the consequence of relaxation, mainly through interactions with the mediating phonons.

4. Crystal-field analysis

The crystal-field model employed here represents a single-ion model based on the scheme of intermediate coupling using the spherical-tensor formalism. Since we are concerned with crystal-field transitions within the ground multiplet, the effect of electronic correlation, which seems to affect only certain electronic states at much higher energies (Pilawa 1991a), is ignored. The Hamiltonian, associated parameters, and underlying assumptions of the theory have been treated in detail elsewhere (Wybourne 1965, Crosswhite and Crosswhite 1984), and only the procedure for the refinement of the crystal-field parameters will be outlined here. The crystal-field part of the Hamiltonian can be written as

$$H_{CF} = \sum_{k,q,i} B_q^k [C_q^k(i) + C_q^k(i)] \qquad k \geqslant q \geqslant 0 \tag{6}$$

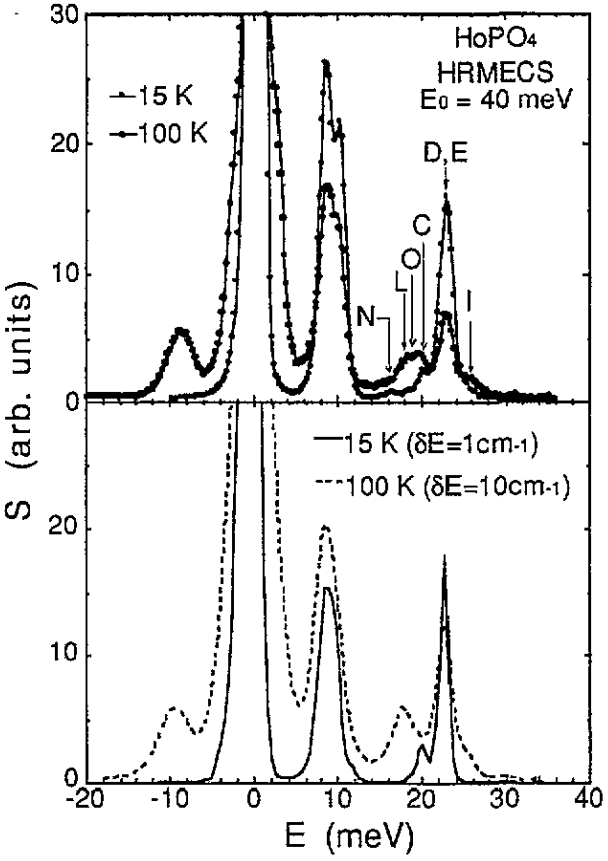

Figure 2. Upper panel: the measured total scattering functions for $HoPO_4$ at 15 and 100 K with neutron incident energy of 40 meV. The curves are guides to the eye. The labelled peaks correspond to crystal-field transitions in figure 6. Lower panel: the calculated scattering functions for crystal-field transitions for $HoPO_4$ at 15 and 100 K. The assumed intrinisic widths of the Lorentzian functions for crystal-field transitions at 15 and 150 K are 1 and 10 cm^{-1}, respectively. The calculated spectra have been convoluted with the instrumental resolution function (see text).

where the $C_q^k(i)$ are spherical tensor operators of rank k and depend on the coordinates of the ith electron. The summation of i is over all f electrons of the ion, and the B_q^k are the crystal-field parameters. The site symmetry at the ion of interest determines which B_q^k parameters are non-zero. For RPO_4 hosts, the rare-earth ions occupy lattice sites of tetragonal (D_{2d}) symmetry, and the crystal-field term is characterized by five real parameters: B_0^2, B_0^4, B_4^4, B_0^6 and B_4^6. It can be shown that the energy-level result is invariant under a simultaneous change of the signs of B_4^4 and B_4^6. The analysis of the inelastic magnetic spectra is carried out using a computer program developed by Crosswhite and Crosswhite (1984). The full Hamiltonian is diagonalized using up to 300 states of the appropriate f^{10} and f^{11} configurations for the Ho^{3+} and Er^{3+} ion, respectively. We have adopted the rare-earth free-ion parameters for R^{3+}: YPO_4 (R = Ho and Er) obtained from optical studies by Edelstein (1986) and Hayhurst *et al* (1981), and these parameters always remained fixed in fitting the neutron data.

The actual refinement of the crystal-field parameters by fitting the observed spectra is relatively straightforward. The initial parameters for $HoPO_4$ and $ErPO_4$ were first obtained by scaling the previously established crystal-field parameters for $TmPO_4$ (Loong *et al* 1993a) according to the radial integrals, $\langle r^k \rangle$, of the rare-earth ions. This method of relating the crystal-field parameters among different isostructural rare-earth compounds has been described previously (Soderholm *et al* 1991, Goodman *et al* 1991) in the crystal-field treatments of rare-earth high-T_c superconductors. Here it was found that the calculated crystal-field-level structure for $HoPO_4$ and $ErPO_4$ using these initial parameter sets already

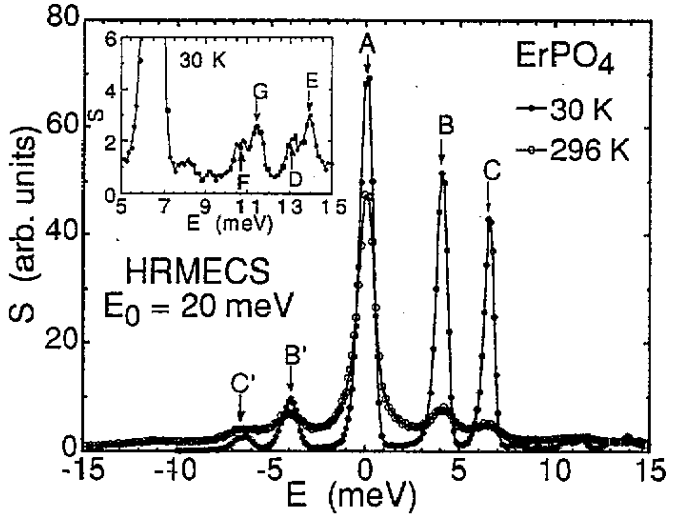

Figure 3. The measured total scattering functions for $ErPO_4$ at 30 and 296 K with neutron incident energy of 20 meV. The curves are guides to the eye. The labelled peaks correspond to crystal-field transitions in figure 7. The peaks at zero energy transfer include nuclear and magnetic elastic scattering. At 30 K the phonon contribution is small but at 296 K a significant diffuse background emerges from phonon scattering. The crystal-field peaks are broadened at high temperatures due to relaxations through interactions with other excitations such as phonons. Inset: the 5–15 meV region at 30 K shown in an expanded scale.

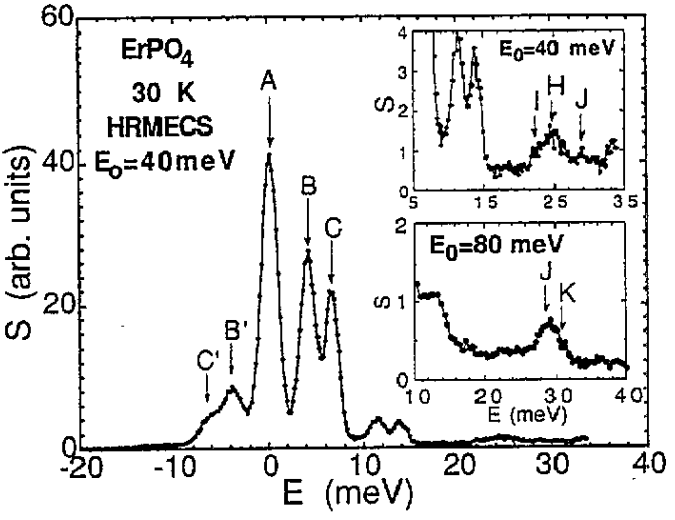

Figure 4. The measured total scattering functions for $ErPO_4$ at 30 K with neutron incident energy of 40 meV. The curves are guides to the eye. The labelled peaks correspond to crystal-field transitions in figure 7. The peaks at zero energy transfer include nuclear and magnetic elastic scattering. Insets: the 5–35 meV region at 30 K with $E_0 = 40$ meV (top) and the 10–40 meV region at 15 K with $E_0 = 80$ meV.

closely resembled the observed excitation spectra. Guided by the selection rules and the assigned states for Ho^{3+} in YPO_4 and $ErPO_4$ obtained from optical studies (Edelstein 1986, Becker *et al* 1985b), subsequent fits to the neutron data of $HoPO_4$ and $ErPO_4$ converged rapidly, yielding calculated energies that were in good agreement with experimental results for all of the transitions. The calculated spectra for $HoPO_4$, using results from the best fit, are shown in the lower panels of figures 1 and 2, and those for $ErPO_4$ in figure 5. The scattering functions $S(Q, E)$ were calculated according to equation (2), except that the delta function was replaced by a Lorentzian function with a width δE. The form factors of the Ho^{3+} and Er^{3+} ions given by Stassis *et al* (1977) were used, and the Debye–Waller factors were set to unity since Q is small. The results were convoluted with the resolution function of the spectrometer (Loong *et al* 1987) and normalized to the observed peaks at 9.8 and 4 meV and 15 K of $HoPO_4$ and $ErPO_4$, respectively (figures 1, 2 and 5). The intrinsic width of an observed crystal-field peak represents a measure of the lifetime of the transition. At elevated temperatures the probability of decay through coupling with other mediating excitations such as phonons increases. As a result, the observed crystal-field peaks have larger widths at high temperatures. The assumed widths of the Lorentzian functions at different temperatures were used for the comparison with the observed spectra and are not necessarily uniform for all the transitions of different energies.

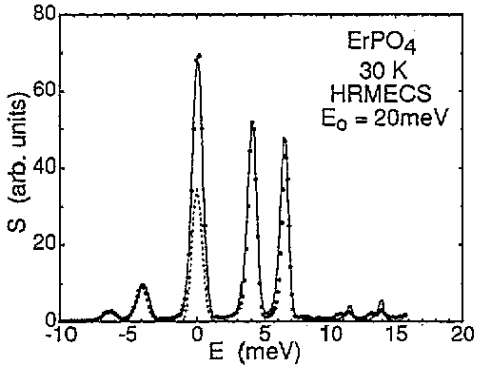

Figure 5. The measured total scattering function (circles) for $ErPO_4$ at 30 K compared with the calculated scattering function (full curve) which includes the calculated crystal-field excitation spectrum and a nuclear elastic-scattering component (dotted curve) (see text).

The calculated spectra, in general, agree well with the experimental results at all temperatures for both $HoPO_4$ and $ErPO_4$. A close inspection of the high-temperature spectra reveals that the broad features are, in fact, composed of several weak unresolved transitions. For example, in $HoPO_4$ the broad peak centred at 2 meV includes the superimposed transitions, F, G, H and J (figure 1) and that at 14 meV includes the N, L and O transitions (figure 2). However, the variation of the integrated intensities of the sharp peaks as well as the unresolved features as a function of temperature (calculated according to equation (2)) agree well with the spectra observed for both $HoPO_4$ and $ErPO_4$. Considering that the calculation has to employ the energies as well as the matrix elements $\langle n|J_\perp|m\rangle$ involving all the states and that it neglects the interactions and/or relaxation of the crystal-field transitions with other elementary excitations such as phonons, the overall agreement between the calculated and the experimental results is good. The derived crystal-field-level schemes and observed transitions for the ground multiplet of $HoPO_4$ and $ErPO_4$ are schematically shown in figures 6 and 7, respectively.

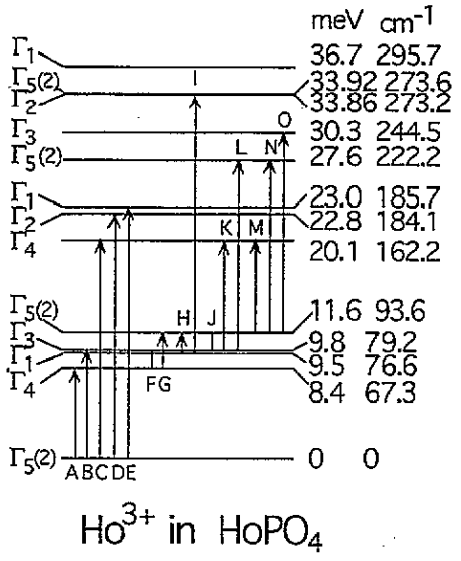

Figure 6. A schematic diagram of the splitting of the Ho^{3+} $^5I_8$ ground multiplet by the crystal field into nine singlets, $3\Gamma_1 + 2\Gamma_2 + 2\Gamma_3 + 2\Gamma_4$, and four doublets, $4\Gamma_5$. The transition labels refer to the experimentally observed transitions shown in figures 1 and 2.

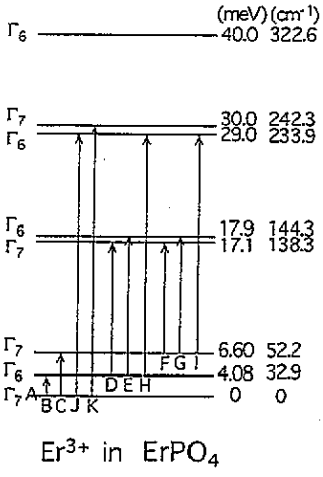

Figure 7. A schematic diagram of the splitting of the Er^{3+} $^4I_{15/2}$ ground multiplet by the crystal field into four Γ_6 and four Γ_7 Kramers doublets. The transition labels refer to the experimentally observed transitions shown in figure 3 and 4.

5. Discussion

5.1. Comparison with optical spectroscopy

In neutron, Raman, and optical spectroscopy of f-electron systems, the main contributions to the cross sections arise from matrix elements of electric-dipole and/or magnetic-dipole operators connecting the participating states. However, the interaction between the magnetic ions with neutron magnetic moments is different from that with the electromagnetic radiation of visible light. For example, the wavelength of the incident photons (10^3–10^6 Å) is much larger than the dimension of the unit cell of crystalline solids, so optical spectroscopy measures electronic excitations and phonons only at Brillouin-zone centre whereas neutrons with wavelengths of ~ 1 Å survey the entire reciprocal space. For measurements of single-ion excitations, both techniques give the same sharp transitions. However, if collective excitations are also involved (e.g. vibronic or electron–phonon interactions), the results could be quite different. Furthermore, the strong photon–atom interaction gives rise to primary

and secondary processes that have to be properly summed over in the calculation of the cross section. The weak scattering of neutrons by magnetic atoms, on the other hand, can afford a simple, first-order treatment based on linear-response theory. Therefore, a comparison of the neutron and optical data often provides complementary information necessary for a more complete characterization of the energy splitting of an f^N configuration ion.

The free-ion and crystal-field parameter sets for pure $HoPO_4$ and for Ho^{3+} ions in a YPO_4 host are listed in table 1. The crystal-field parameters for $HoPO_4$ obtained from fitting the neutron data with fixed free-ion parameters for Ho^{3+} in YPO[4] are given in the third column, and those obtained from fitting both the neutron data and the high-energy states of $^5I_7$, $^5I_6$ and $^5I_5$ multiplets obtained from polarized absorption spectroscopy by Bischoff *et al* (1991) are in the fourth column. Only the Slater–Condon electrostatic parameters, F^2, F^4 and F^6, in addition to the crystal-field parameters, are varied in the later analysis since other parameters have little effect on the results of the fits. It can be seen that the crystal-field parameter sets for $HoPO_4$ obtained in the present analyses agree well with those of Bischoff *et al* (1991) obtained from optical spectroscopy. The calculated Ho energy levels using the two parameter sets for $HoPO_4$ (table 1), together with the observed energies from neutron ($HoPO_4$) and optical ($HoPO_4$ and Ho in YPO_4) studies, are given in table 2. The agreement between the observed and calculated energies of $HoPO_4$ ^5I multiplets is good and the root-mean-square energy deviation is 3.2 cm^{-1}. The $\sim$ 10% changes in F^2, F^4 and F^6 do not seriously affect the positions and intensities of the low-lying states in the ground multiplet, as was observed previously in the case of $TmPO_4$ (Loong *et al* 1993a). The calculated energies for the $^3K_7$ and $^3H_6$ states, on the other hand, differ systematically from those measured by Enderle *et al* (1990). For example, the calculated centre of gravity of the $^4K_7$ term is 26 025.6 cm^{-1} as compared to the observed value of 26 164.2 cm^{-1}, and similar effects are found for the $^3H_6$ term. Similar discrepancies involving the high-energy states have also been observed in other Ho^{3+} systems (Rajnak and Krupke 1967, Crosswhite *et al* 1977) and are attributed to effects of electronic correlation on the crystal field that are not considered in the one-electron crystal-field Hamiltonian in equation (6). This problem has recently been investigated by Pilawa (1991a, b, c). Significant improvements in the fits to data ranging from 0 to 28 000 cm^{-1} for Ho^{3+} in the hosts of YVO_4, $YAsO_4$, and $HoPO_4$ have been achieved by the introduction of additional (L, S)-term-dependent crystal-field parameters.

Electronic Raman scattering for rare-earth ions in solids involves $|4f^N, \Gamma_n) \rightarrow |4f^N, \Gamma_k)$ transitions via virtual intermediate states. Both one- and two-photon scattering events are common in experiments using laser radiation. The scattering amplitude obtained from second-order perturbation theory contains an intractable sum over the complex intermediate states such as the $|4f^{N-1}, \beta)(\beta = 5d, g)$ states and states in the continuum d and g configurations. The Judd–Ofelt approximation (Judd 1962, Ofelt 1962), which employs a closure relation to perform a piecewise summation over subgroups of *non-interacting* intermediate states, has been quite successful in the analysis of the optical data of many rare-earth systems. Becker *et al* (1985b) reported the energies of the four lowest crystal-field levels of $ErPO_4$ from electronic Raman-scattering experiments. In a later report Becker *et al* (1986) noted that the spectral line at 488.0 nm of an argon-ion laser nearly coincides with the excitation energy from the Er^{3+} ground state to the lowest Γ_7 crystal-field state of the $^4F_{7/2}$ multiplet. The scattering amplitudes connecting the ground state to the low-lying excited states are enhanced significantly by the resonant channels corresponding to excitations from the ground state to the intermediate $^4F_{7/2}$ crystal-field levels. As a result, all of the energy levels within the ground multiplet of $ErPO_4$ have been measured by resonant electronic Raman scattering.

Table 1. The free-ion and crystal-field parameter sets (cm^{-1}) for Ho^{3+} in YPO_4 and pure $HoPO_4$.

Parameters	Ho^{3+} in YPO_4[a]	$HoPO_4$[b]	$HoPO_4$[c]
F^2	93668	93668	96243
F^4	66113	66113	67817
F^6	49372	49372	45968
α	18.9	18.9	18.9
β	−611.0	−611.0	−611.0
γ	2013.0	2013.0	2013.0
ζ	2134	2134	2134
T^2	248.6	248.6	248.6
T^3	37.0	37.0	37.0
T^4	98.0	98.0	98.0
T^6	−316.0	−316.0	−316.0
T^7	440.0	440.0	440.0
T^8	372.0	372.0	372.0
M^0	3.0	3.0	3.0
M^2	1.7	1.7	1.7
M^4	1.1	1.1	1.1
P^2	528.0	528.0	528.0
P^4	396.0	396.0	396.0
P^6	264.0	264.0	264.0
B_0^2	352	402	374 (372)
B_0^4	67	41	60 (26)
B_4^4	−673	−683	−662 (−639)
B_0^6	−757	−718	−726 (−760)
B_4^6	−3.7	−52	−57 (−29)

[a] From optical study of Ho^{3+} in YPO_4 by Edelstein (1986).

[b] Using the free-ion parameters for Ho^{3+} in YPO_4 of Edelstein (1986) to fit neutron data of $HoPO_4$.

[c] From a refinement of the F^2, F^4, F^6 and crystal-field parameters by fitting the neutron data and optical data given by Bischoff *et al* (1991) for $HoPO_4$. The crystal-field parameters in parentheses are given by Bischoff *et al* (1991) from an analysis of the infrared absorption spectra of the $^5I_7$, $^5I_6$ and $^5I_5$ terms.

The free-ion crystal-field parameter sets for pure $ErPO_4$ and for Er^{3+} in YPO_4 are listed in table 3. Only the crystal-field parameters were varied in the fits to the neutron data. The calculated energy levels of the Er^{3+} $^4I_{15/2}$ ground multiplet are compared with the neutron and Raman data in table 4. The crystal-field-level scheme for the Er^{3+} $^4I_{15/2}$ ground multiplet as determined by the INS study (figure 7) agrees with that obtained from optical spectroscopy (Becker *et al* 1985b, 1986, Williams *et al* 1989) except for two energy levels, i.e. the third Γ_7 state (neutron: 17.1 meV, Raman: 13.0 meV) and the highest Γ_6 state (neutron: 40 meV, Raman: 33.4 meV). The calculated position of the highest Γ_6 state was 40 meV, but excitations to this state were not observed in the neutron-scattering experiment because of the very small matrix elements. An attempt to assign the third Γ_7 state at 13 meV (as in the optical data analysis) did not yield a good fit to the overall neutron data. The excitations from the ground state to the first two levels (the Γ_6 state at 4.08 and the Γ_7 state at 6.60 meV) are by far the most intense features in the neutron and in the resonance and non-resonance Raman scattering (Becker *et al* 1985b, 1986) experiments, and they are in excellent agreement. Transitions to the third Γ_7 state at 13.0 meV in the Raman spectra were weak and were observed only along the incident- and scattered-phonon polarization parallel to the crystallographic *c*-axis. A direct comparison of the observed

Table 2. The calculated and observed energies of pure $HoPO_4$ and Ho^{3+} in YPO_4.

	E^{calc} (cm^{-1})		E^{obs} (cm^{-1})		
States	$HoPO_4$[a]	$HoPO_4$[b]	$HoPO_4$[c]	$HoPO_4$[d]	Ho^{3+} in YPO_4[e]
$^5I_8$					
Γ_5	0.0	0.0	0.0	—	0.0
Γ_4	67.3	67.3	66.1	—	66.6
Γ_1	76.6	73.5	—	—	71.7
Γ_3	79.2	79.6	80.7	—	80.9
Γ_5	93.6	91.4	94.0	—	89.2
Γ_4	162.2	161.7	162.1	—	160.4
Γ_2	184.1	185.6	184.3	—	188.1
Γ_1	185.7	187.2	184.3	—	—
Γ_5	222.2	222.7	—	—	—
Γ_3	244.5	239.9	244.4	—	250.2
Γ_2	273.2	273.8	—	—	279.3
Γ_5	273.6	270.7	—	—	—
Γ_1	295.7	294.2	—	—	—
$^5I_7$					
Γ_3	—	5152.1	—	5152.5	5153.2
Γ_4	—	5157.4	—	5158.5	5155.8
Γ_5	—	5164.9	—	5164.7	—
Γ_2	—	5170.7	—	5170.3	—
Γ_5	—	5171.4	—	5172.1	—
Γ_3	—	5203.0	—	5203.5	—
Γ_5	—	5210.0	—	5211.4	—
Γ_1	—	5218.9	—	5220.4	—
Γ_2	—	5261.1	—	5264.2	—
Γ_5	—	5262.3	—	5266.2	5264.5
Γ_4	—	5262.5	—	5264.2	—
$^5I_6$					
Γ_4	—	8648.5	—	8650.3	—
Γ_3	—	8649.4	—	8650.3	—
Γ_1	—	8672.8	—	8673.5	—
Γ_5	—	8673.4	—	8674.1	8670.7
Γ_4	—	8680.6	—	8681.9	—
Γ_2	—	8689.8	—	8690.3	—
Γ_5	—	8702.4	—	8703.4	8708.4
Γ_3	—	8737.1	—	—	—
Γ_5	—	8750.5	—	8750.1	8746.5
Γ_1	—	8759.0	—	8759.0	—
$^5I_5$					
Γ_5	—	11212.1	—	11215.9	—
Γ_5	—	11231.3	—	11234.5	—
Γ_3	—	11238.0	—	11244.6	—
Γ_2	—	11249.3	—	11253.0	—
Γ_1	—	11261.3	—	11262.0	—
Γ_4	—	11284.7	—	11279.6	—
Γ_5	—	11292.5	—	11290.7	—
Γ_2	—	11309.5	—	11306.9	—

[a] Result of fitting the neutron data only.
[b] Result of fitting the neutron (this work) and optical (Enderle *et al* 1990) data.
[c] This work.
[d] Optical data from Enderle *et al* (1990).
[e] Optical data from Edelstein (1986).

Table 3. The free-ion and crystal-field parameter sets (cm^{-1}) for Er^{3+} in YPO_4 and pure $ErPO_4$.

Parameters	Er^{3+} in YPO_4[a]	$ErPO_4$[b]
F^2	97058	97058
F^4	69142	69142
F^6	48232	48232
α	15.9	15.9
β	632.0	632.0
γ	2017.0	2017.0
ζ	2368	2368
T^2	157.5	157.5
T^3	48.0	48.0
T^4	18.0	18.0
T^6	−342.0	−342.0
T^7	214.0	214.0
T^8	449.0	449.0
M^0	4.5	4.5
M^2	2.52	2.52
M^4	1.71	1.71
P^2	667.0	667.0
P^4	500.3	500.3
P^6	333.5	333.5
B_0^2	279	390
B_0^4	155	114
B_4^4	−756	−711
B_0^6	−537	−697
B_4^6	−141	−62

[a] From optical study of Er^{3+} in YPO_4 by Hayhurst *et al* (1981).
[b] The free-ion parameters for Er^{3+} in YPO_4 were used and fixed in the fits of the neutron data of $HoPO_4$.

Table 4. The calculated and observed energies of pure $ErPO_4$.

		$E^{obs}(cm^{-1})$		
States	$E^{calc}(cm^{-1})$	Neutron This work	Resonance Raman[a]	Non-resonance Raman[b]
Γ_7	0.0	0	0	0
Γ_6	32.9	32.9	33	33
Γ_7	52.2	52.2	53	53
Γ_7	138.2	138.2	105	105
Γ_6	144.3	144.3	145	145
Γ_6	233.9	233.9	234	—
Γ_7	242.3	—	246	—
Γ_6	322.6	—	269	—

[a] Becker *et al* (1986).
[b] Becker *et al* (1985b).

Raman intensities and polarization patterns with calculations based on the Judd–Ofelt theory has not been satisfactory (Becker *et al* 1985a, b, Williams *et al* 1989). At present, the reason for the disagreement for these two energy levels between the neutron and optical studies is not known. We have accepted the present assignment because the calculated spectra agree well with all of the observed neutron data; the crystal-field parameters are consistent with those for $TmPO_4$ through a scaling of the different rare-earth 4f radial wavefunctions. The

calculated magnetic susceptibility, as compared to that using the CF parameters (Hayhurst *et al* 1981) obtained from the optical data of Er-doped YPO_4, is in better agreement with the experimental susceptibility data.

5.2. Magnetic properties

At low temperatures, only the lowest crystal-field states of the rare-earth ions are populated. The symmetry and the magnetization of these states directly affect the ion–ion and ion–lattice interactions. Consequently, the occurrence of various magnetic effects and/or cooperative transformations varies among different members across the RPO_4 series. $HoPO_4$ orders antiferromagnetically in a simple two-sublattice structure with the Ho magnetic-moment direction parallel to the crystallographic optical axis (the *c*-axis) at a Néel temperature T_N of 1.39 K (Cooke *et al* 1973, Laugsch *et al* 1975, Millhouse *et al* 1979). This spin structure is common to many RMO_4 (M = P, V, As) compounds such as $DyPO_4$ (T_N = 3.4 K), $TbPO_4$ (T_N = 2.2 K) and $GdVO_4$ (T_N = 2.5 K) and can be described in terms of Ising-like interactions (Bleaney 1988). Neutron diffraction and susceptibility measurements by Kockelmann *et al* (1991) on $ErPO_4$ revealed no magnetic ordering down to 0.4 K. The low Néel temperature indicates a small exchange energy for rare-earth ion–ion (indirect) interactions compared to the overall crystal-field splitting, and one may gain significant insight into the nature of the magnetic interactions by considering the anisotropic magnetization distribution of only the low-lying crystal-field states.

Some aspects of the anisotropy of the magnetic susceptibility should be emphasized. Neutron magnetic scattering provides a measure of the imaginary part of the dynamic magnetic susceptibility of the system which can be converted to the static susceptibility by the Kramers–Kronig relation. Since the neutron-scattering experiments were conducted at only a few different temperatures, we have chosen to compare the static magnetic susceptibility calculated according to the van Vleck (1932) formalism (using the crystal-field states derived from neutron scattering) with the bulk susceptibility obtained from single-crystal measurements instead of the Kramers–Kronig analysis. Good agreement between the calculated and observed paramagnetic susceptibility over a wide range of temperatures should also lend credence to the correctness of the crystal-field analysis. Figure 8 shows the calculated and measured paramagnetic susceptibility of $HoPO_4$ with the magnetic field parallel and perpendicular to the crystallographic *c*-axis. The agreement between the calculated and observed susceptibility is excellent over the temperature range of 5–300 K. The susceptibility data agree with those reported by Neogy *et al* (1989) except that four data points of $\chi_\parallel$ between 4 and 20 K (inset of figure 1 of Neogy *et al* 1989) are significantly smaller than the present data. In order to explain these particular data points, Neogy *et al* had to invoke exchange effects in addition to the crystal-field treatment. We suspect that these data in the 4–20 K region are incorrect for the following reasons: (i) exchange effects were introduced at temperatures 5–10 times higher than the Néel temperature without a measurable contribution from exchange interactions in the specific-heat data at these temperatures; and (ii) in a similar analysis of the susceptibility data of $TbPO_4$, Sen *et al* (1988) found that exchange effects are only needed a few degrees above the Néel temperature. The crystal-field levels of $HoPO_4$ predicted by Neogy *et al* (1989), in general, differ from our observed energies by more than 10 cm^{-1}.

The susceptibility of $HoPO_4$ is highly anisotropic at temperatures below 50 K, approaching a $\chi_\parallel/\chi_\perp$ of 45 at 5 K. This effect arises from the fact that the Γ_5 ground doublet is made up of 98% of $|8, \pm 7\rangle$ states, forming a large magnetization density along the *c*-axis. The spectroscopic splitting factors $g_\parallel$ and $g_\perp$ for the Γ_5 doublet are 17.2 and 0, respectively, which is in good agreement with those from Zeeman-effect measurements

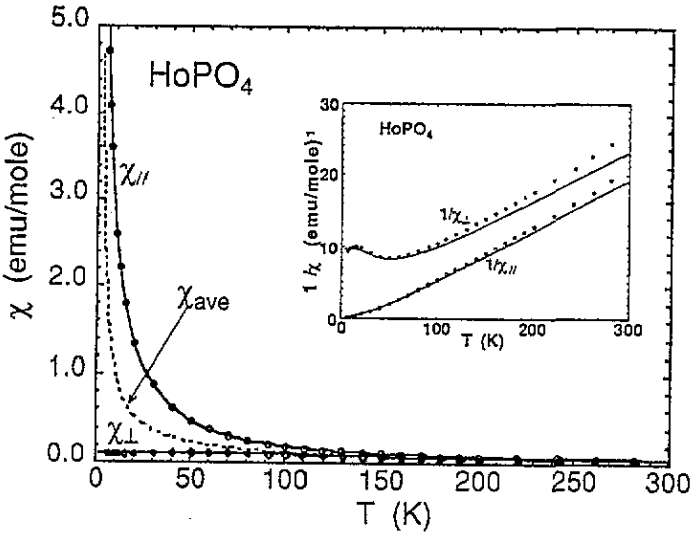

Figure 8. The calculated (curves) and measured (symbols) paramagnetic susceptibility of $HoPO_4$ with the field directions perpendicular ($\chi_\perp$) and parallel ($\chi_\parallel$) to the crystallographic c-axis. χ_{ave} is the powder-averaged susceptibility. Inset: the inverse susceptibility of $HoPO_4$.

($g_\parallel = 16.2 \pm 0.2$, Cooke *et al* 1973) measurements. The calculated saturated moment for the Γ_5 doublet is 8.6 μ_B which agrees well with the magnetic moment on the two Ho antiferromagnetic sublattices as determined by neutron diffraction (Millhouse *et al* 1979). The good agreement between the calculated *single-ion* paramagnetic susceptibility and the experimental data down to 5 K indicates that the strength of the Ho ion–ion exchange interaction is comparable to the dipole–dipole interaction of the saturated moments, which is also confirmed by an analysis of the specific heat at the magnetic phase transition (Laugsch *et al* 1975). Encouraged by the consistency of the results indicating a dominant role of the Γ_5 ground state as a precursor to the magnetic phase transition, an estimate was made of the effective exchange field for intersite interactions using the simple relations between the crystal and molecular fields $\lambda\chi^0 = 1$ and $H_{ex} = \lambda M_0$, where χ^0 is the calculated susceptibility at T_N due to crystal-field effects alone, M_0 is the saturated magnetization of the Γ_5 state, and λ is the molecular-field parameter (Bleaney 1963). Using the values of $\chi^0 = 19.77$ emu/mole and $M_0 = 8.6$ μ_B/Ho ion, we find an effective exchange field of $H_{ex} = 2.43$ kOe, which compares well with that (2.05 kOe) estimated from the specific-heat analysis by Laugsch *et al* (1975).

The above results suggest that the Ho magnetic ground state plays an important role as a 'bootstrap' for the long-range ordering of the Ho moments at low temperatures. The resulting ordered moments are parallel to the easy axis of the susceptibility. The simplicity of the dipole and exchange interactions of the Ho moments supports the description of the antiferromagnetic ordered phase by means of a three-dimensional Ising model.

If $ErPO_4$ orders at all, such an ordering apparently only occurs at a much lower temperature. ($ErVO_4$ was thought to order at 0.4 K, Metcalfe and Rosenberg (1972). More recently, an incommensurate magnetic structure of $ErVO_4$ was observed at $T < 3$ K by Kockelmann *et al* (1991).) The magnetic properties of the low-lying crystal-field states of the Er^{3+} ion should provide an explanation for this phenomenon. The calculated and observed paramagnetic susceptibilities of $ErPO_4$, as shown in figure 9, agree well over the temperature range of 5–300 K. The calculated and observed susceptibilities for a powder sample of $ErPO_4$ also agree with the measurements reported by Will *et al* (1971). In contrast to the highly anisotropic behaviour of $HoPO_4$ at low temperatures, $\chi_\perp$ is larger than $\chi_\parallel$ in $ErPO_4$ primarily between 10 and 100 K, and as the temperature drops below

contrast to the highly anisotropic behaviour of $HoPO_4$ at low temperatures, $\chi_\perp$ is larger than $\chi_\parallel$ in $ErPO_4$ primarily between 10 and 100 K, and as the temperature drops below about 10 K, $\chi_\parallel$ and $\chi_\perp$ become comparable in magnitude, showing no apparent 'easy direction' for cooperative magnetization. The relatively isotropic susceptibility at $T < 10$ K is a consequence of the close-to-spherical magnetization densities of the low-energy states, which can be seen from the g-factors, $g_\parallel$ and $g_\perp$, for the first three Kramers doublets, Γ_7 (0 meV), Γ_6 (4.1 meV), and Γ_7 (6.6 meV), being (6.6, −4.6), (−3.6, −7.7), (−8.4, 4.3) and (17.4, 0.10), respectively. The coupling of the saturated moments and precursor exchange fields along any preferred direction is less effective in $ErPO_4$ than in $HoPO_4$, resulting in the persistence of the paramagnetic phase for $ErPO_4$ at low temperatures.

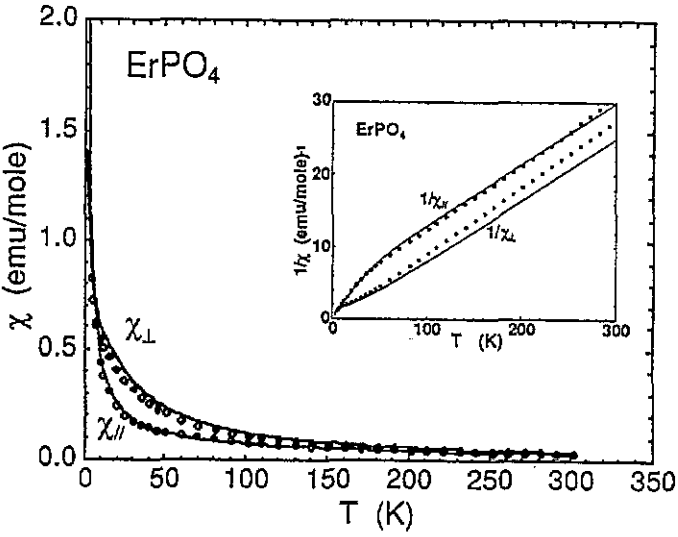

Figure 9. The calculated (curves) and measured (symbols) paramagnetic susceptibility of $ErPO_4$ with the field directions perpendicular ($\chi_\perp$) and parallel ($\chi_\parallel$) to the crystallographic c-axis. Inset: the inverse susceptibility of $ErPO_4$.

Various analyses of the polycrystalline magnetic susceptibility, hyperfine interaction, and EPR data for $ErPO_4$ and Er^{3+} in zircon-structure hosts have been made in an attempt to understand the crystal-field-level structure (Will *et al* 1971, Vishwamittar and Puri 1974). Only a partial resolution of certain levels and some of the magnetic properties of the wavefunctions were possible. The crystal-field parameters thus obtained exhibit significant uncertainty. We have shown here that neutron and optical spectroscopy are the best methods for characterizing the rare-earth energy levels and the ground-state properties of these materials.

Finally, we have shown that the calculated contribution of the crystal-field states to the specific heat of $HoPO_4$ and $ErPO_4$ (see figure 10). The Schottky-like peaks present near 70 K (for $HoPO_4$) and at 25 and 80 K (for $ErPO_4$) are the result of low-lying crystal-field states. The analysis indicates that care should be taken so that the rare-earth crystal-field contribution is accounted for in an interpretation of the measured total specific-heat data for both compounds.

In conclusion, the static and dynamic magnetic response of pure $HoPO_4$ and $ErPO_4$ have been investigated using neutron spectroscopy and single-crystal magnetic susceptibility measurements. We have demonstrated that a combined treatment of the neutron and optical data provides complementary information that is necessary for a proper characterization of the energy level splitting and wavefunctions of the rare-earth ions in these materials.

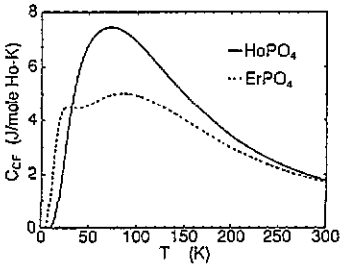

Figure 10. *The calculated contributions to the specific* heat from the rare-earth ion crystal-field states for $HoPO_4$ and $ErPO_4$.

Crystal-field analyses of the neutron data have satisfactorily accounted for the observed spectra at all temperatures and led to further refinements of the crystal-field parameters for both compounds. However, we find a discrepancy (for which we have no explanation) in the energies of two crystal-field levels in $ErPO_4$ as measured by resonant electronic Raman scattering and determined by fitting the inelastic neutron scattering data. We find that the crystal-field-level structure derived here can provide a basis for explaining the low-temperature rare-earth magnetic properties. The calculated paramagnetic susceptibilities for $HoPO_4$ and $ErPO_4$ agree well with the experimental data. The highly anisotropic, saturated magnetization of the ground doublet of $HoPO_4$ favours a coupling with exchange interactions for magnetic ordering at low temperature, whereas the nearly spherical symmetric moments in the low-lying Kramers doublets of $ErPO_4$ would be ineffective for long-range magnetic ordering. The spectroscopic splitting g-factors of the doublet states, the saturated moments at low temperatures, and the estimated effective exchange field (for $HoPO_4$) are in good agreement with the values obtained by other workers from specific-heat, hyperfine interaction, and neutron diffraction experiments

Acknowledgments

We thank Dr G L Goodman for helpful discussions and Dr J W Richardson Jr for his assistance in the neutron powder diffraction experiments. Work performed at Argonne, Oak Ridge and Lawrence Berkeley Laboratories is supported by the US DOE, Office of Basic Energy Sciences, Chemical Sciences and Materials Sciences Divisions under Contracts W-31-109-ENG-38 (ANL), DE-AC05-84OR21400 (ORNL), and DE-AC03-76SF00098 (LBL), respectively.

References

Abraham M M, Boatner L A, Quinby T C, Thomas D K and Rappaz M 1980 *Radioact. Waste Management* **1** 181–91

Becker P C, Edelstein N, Judd B R, Leavitt R C and Lister G M S 1985a *J. Phys. C: Solid State Phys.* **18** L1063

Becker P C, Edelstein N, Williams G M, Bucher J J, Russo R E, Koningstein J A, Boatner L A and Abraham M M 1985b *Phys. Rev.* B **31** 8102–10

Becker P C, Edelstein N, Williams G M, Koningstein J A, Boatner L A and Abraham M M 1992 *Phys. Rev.* B **45** 5027–5030

Becker P C, Hayhurst T, Shalimoff G, Conway J G, Edelstein N, Boatner L A and Abraham M M 1984 *J. Chem. Phys.* **81** 2872–8

Becker P C, Williams G M, Russo R E, Edelstein N, Koningstein J A, Boatner L A and Abraham M M 1986 *Optics Lett.* **11** 282–4

Bischoff H, Pilawa B, Kasten A and Kahle H G 1991 *J. Phys.: Condens. Matter* **3** 10057–64

Bleany B 1963 *Proc. Soc.* A **276** 19–27
—— 1988 *Handbook on the Physics and Chemistry of Rare Earths* vol 11, ed K A Gschneidner Jr and L Eyring (Amsterdam: Elsevier) ch 77, pp 323–407
Boatner L A, Beall G W, Abraham M M, Finch C B, Floran R J, Huray P G and Rappaz M 1981 *Management of Alpha-Contaminated Wastes* IAEA-SM-246/73 (Vienna: IAEA) pp 411–22
Boatner L A, Beall G W, Abraham M M, Finch C B, Huray P G and Rappaz M 1980 *Scientific Basis for Nuclear Waste Management* vol II, ed C J Northrup (New York: Plenum) pp 289–96
Cooke A H, Swithenby S J and Wells M R 1973 *J. Phys. C: Solid State Phys.* **6** 2209–16
Crosswhite H M and Crosswhite H 1984 *J. Opt. Soc. Am.* B **1** 246–54
Crosswhite H M, Crosswhite H, Edelstein N and Rajnak K 1977 *J. Chem. Phys.* **67** 3002–10
De Jongh L J and Miedema A R 1974 *Adv. Phys.* **23** 1–260
Edelstein N 1986 in Becker P C *PhD thesis, Lawrence Berkeley Laboratory Report* LBL-22634, p 255
Enderle M, Pilawa B and Kahle H G 1990 *J. Phys.: Condens. Matter* **2** 4711–15
Goodman G L, Loong C-K and Soderholm L 1991 *J. Phys.: Condens. Matter* **3** 49–67
Hayhurst T, Shalimoff G, Edelstein N, Boatner L A and Abraham M M 1981 *J. Chem. Phys.* **74** 5449–52
Hikichi Y and Nomura T 1987 *J. Am. Ceram. Soc.* **70** C-252–3
Judd B R 1962 *Phys. Rev.* **127** 750–61
Kockelmann W, Schäfer and Will G 1991 *Eur. J. Solid State Inorg. Chem.* **28** 515–8
Laugsch J, Kahle H G, Schwab M and Wüchner W 1975 *Physica* B **80** 269–86
Lee J N, Moos H W and Mangum B W 1971 *Solid State Commun.* **9** 1139–41
Loong C-K, Ikeda S and Carpenter J M 1987 *Nucl. Instrum. Methods* A **260** 381–402
Loong C-K and Soderholm L 1992a *High Temperature Superconductivity: Physical and Mechanical Properties* ed S K Malik and S S Shah (Nova) at press
—— 1992b *Phys. Rev.* to be published
Loong C-K, Soderholm L, Abraham M M, Boatner L A and Edelstein N 1993a *J. Chem. Phys.* **98** 4214–22
Loong C-K, Soderholm L, Hammonds J P, Abraham M M, Boatner L A and Edelstein N 1993b *J. Appl. Phys.* **73** 6069–71
Lovesey S W 1984 *Theory of Neutron Scattering from Condensed Matter* vol 2 (Oxford: Oxford University Press)
Metcalfe M J and Rosenberg H M 1972 *J. Phys. C: Solid State Phys.* **5** 474–80
Millhouse A H, Steiner M and Dachs H 1979 *J. Appl. Phys.* **50** 2011-13
Milligan W O, Mullica D F, Beall G W and Boatner L A 1983a *Inorg. Chim. Acta* **70** 133–6
—— 1983b *Acta Crystallogr.* C **39** 23–4
Neogy D, Sen H and Wanklyn B M 1989 *J. Magn. Magn. Mater.* **78** 387–92
Ofelt G S 1962 *J. Chem. Phys.* **37** 511–20
Pilawa B 1991a *J. Phys.: Condens. Matter* **3** 655–66
—— 1991b *J. Phys.: Condens. Matter* **3** 4293–6
—— 1991c *J. Phys.: Condens. Matter* **3** 667–73
Rajnak K and Krupke W 1967 *J. Chem. Phys.* **46** 3532–42
Sen H, Neogy D and Wanklyn B M 1988 *J. Magn. Magn. Mater.* **73** 221–8
Soderholm L, Loong C-K, Goodman G L and Dabrowski B D 1991 *Phys. Rev.* B **43** 7923–35
Soderholm L, Loong C-K and Kern S 1992 *Phys. Rev.* B **45** 10062–70
Sokolov V I, Kazei Z A and Kolmakova N P 1992 *Physica* B **176** 101–12
Sokolov V I, Kazei Z A, Kolmakova N P and Solov'yanova T V 1991 *Sov. Phys.–JETP* **73** 524–33
Stassis C and Deckman H W 1975 *Phys. Rev.* B **12** 1885–98
—— 1976 *J. Phys. C: Solid State Phys.* **9** 2241–60
Stassis C, Deckman H W, Harmon B N, Desclaux J P and Freeman A J 1977 *Phys. Rev.* B **15** 369–76
van Vleck J H 1932 *The Theory of Electric and Magnetic Susceptibilities* (London: Oxford University Press)
Vishwamittar and Puri S P 1974 *Phys. Rev.* B **9** 4673–89
Will G, Lugscheider W, Zinn W and Patscheke E 1971 *Phys. Status Solidi* b **46** 597–601
Williams G M, Becker P C, Edelstein N, Boatner L A and Abraham M M 1989 *Phys. Rev.* B **40** 1288–96
Wright J C and Moss H W 1969 *Phys. Lett.* **29A** 495–6
Wybourne B G 1965 *Spectroscopic Properties of Rare Earths* (New York: Wiley)